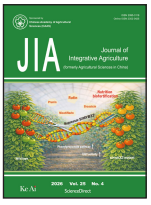
Journal of Integrative Agriculture 2026, 25(4): 1475–1487

Available online at ScienceDirect

Journal of Integrative Agriculture



RESEARCH ARTICLE

The *TEI* (*Tomato Elongated Internode*) gene encodes a GA20ox protein conferring internode elongation in tomato

Xinyi Jia[1], Hexuan Wang[1], Chunying Feng[1], Xinyi Zhang[1], Guohao Yang[1], Ping Zhang[1], Qingjun Fu[1], Te Wang[1], Jingfu Li[1], He Zhang[1], Jingbin Jiang[1], Ke Wen[2], Xiangyang Xu[1#], Huanhuan Yang[1#]

[1] *College of Horticulture and Landscape Architecture, Northeast Agricultural University, Harbin 150030, China*
[2] *Sanya Research Institute, Hainan Academy of Agricultural Sciences, Sanya 572000, China*

Highlights

- *TEI* was identified as the gibberellin 20-oxidase (*GA20ox*) gene, regulating the internodes of tomatoes.
- *TEI* gene regulates cell elongation by influencing the content of endogenous gibberellins, and affects the elongation of tomato internodes.

Abstract

The ideal plant architecture is a critical factor in achieving high yields in tomato (*Solanum lycopersicum*) cultivation. The length and number of internodes directly influence plant height. Therefore, investigating the regulatory mechanisms of internode morphology is essential for the genetic enhancement of tomatoes. We identified a naturally occurring field mutant, *tomato elongated internode* (*tei*), characterized by longer internodes and darker leaf color. Physiological hormone and microscopic studies revealed that, compared to wild-type (WT) plants, the *tei* mutant exhibited increased endogenous GA3 levels, enhanced photosynthetic capacity, and elongation of stem internode cells. RNA-seq analysis results of *tei* and WT indicated enrichment in the gibberellin pathway. We employed BSA-seq for mapping analysis on *tei*, WT, and F_2 populations, leading to the fine mapping of the candidate gene designated as *TEI* (*Tomato Elongated Internode*). This gene encoded a gibberellin 20 oxidase (GA20ox) protein and was identified as *Solyc09g042210*. Additionally, we discovered numerous SNPs and InDel mutations in the *TEI* promoter region, with expression levels of *TEI* in *tei* stems significantly higher than those in WT. Furthermore, knocking out the *TEI* gene eliminated its role in elongating internodes. We proposed that *TEI* serves as the primary effector gene regulating the internode elongation phenotype associated with *tei*. This discovery offered researchers a novel target for enhancing crop plant varieties by modulating gibberellin homeostasis, ultimately contributing to the breeding of superior tomato varieties.

Keywords: internode elongation, gibberellins, BSA-seq, fine mapping, tomato

1. Introduction

Strategies aimed at enhancing the yields of crops such as rice and wheat through the optimization of plant architecture have garnered significant attention (Yan *et al.* 2022). Plant height, particularly the length of stem internodes, directly influences the photosynthetic efficiency and biomass accumulation of these crops (Gao *et al.* 2018; Fang *et al.* 2019). The early 20th century saw the application of the wheat dwarf gene *Rht* and the rice semi-dwarf gene *sd1*, which were pivotal to the success of the "Green Revolution" (Khush 1999, 2001; Berry *et al.* 2004). To date, over 60 recessive dwarf mutants and more than 10 recessive semi-dwarf mutants have been identified in rice, with some characterized in detail (Li *et al.* 2017). Additionally, maize (*ZmGA20ox3*, *ZmGA20ox5*), soybean (*dw1*), and *sorghum bicolor* (*dw1-dw4*) have been identified as key genes regulating internode length (Yamaguchi *et al.* 2016; Gao *et al.* 2018; Paciorek *et al.* 2022). Consequently, the identification of genes that regulate internode length, along with the elucidation of their genetic patterns and molecular mechanisms, not only

Received 2 December 2024; Received in revised form 16 September 2025; Accepted 17 November 2025; Available online 29 December 2025
Xinyi Jia, E-mail: jia593718265@163.com; #Correspondence Xiangyang Xu, E-mail: xuxyneau@gmail.com; Huanhuan Yang, E-mail: huanyaya0126@sina.com

© 2026 CAAS. Publishing services by Elsevier B.V. on behalf of KeAi Communications Co. Ltd. This is an open access article under the CC BY-NC-ND license (http://creativecommons.org/licenses/by-nc-nd/4.0/). Peer review under responsibility of Editorial Board of *Journal of Integrative Agriculture*.
doi: 10.1016/j.jia.2025.12.055

enriches our understanding of the regulatory mechanisms of plant development but also holds promise for optimizing the morphology of various crops, including tomato plants.

The regulation of plant height is closely associated with the biosynthesis and signaling of endogenous plant hormones, particularly gibberellins (GAs) (Wang and Wang 2022). GAs are diterpenoid phytohormones that play a crucial role in various plant functions, including stem elongation, root growth, fruit and flower development, seed germination, and leaf expansion (Olszewski *et al.* 2002; Li *et al.* 2017). Understanding the synthesis and regulation of GAs is essential for elucidating their roles in plant growth and development. The synthesis of GA begins with *trans*-geranylgeranyl diphosphate (GGPP), which undergoes a series of biological reactions to be ultimately converted into the biologically active forms GA1 or GA4 (Zhang *et al.* 2011). This process involves three types of enzymes: terpene cyclases (*TPS*), monooxygenases characterized by cytochrome P450s (*P450s*), and 2-oxoglutarate-dependent dioxygenases (*2ODD*) (Yamaguchi *et al.* 2016). Research conducted on several crops, including Arabidopsis, rice, soybean (Xue *et al.* 2008; Kieffer *et al.* 2011), and wheat has demonstrated that GAs are key phytohormones in regulating stem elongation and overall plant height (Magome *et al.* 2004; Ji *et al.* 2014). Plants deficient in GA synthesis typically exhibit shorter internodes and display dwarfism. For instance, mutations in the *oscps1* gene in rice lead to significantly dwarfed plants (Ishikawa *et al.* 2005). In *Arabidopsis thaliana*, the overexpression of the NAC-like protein GSF induces dwarfism by reducing the level of GA synthesis through the upregulation of *AtGA2ox2* and *AtGA2ox6* (Chen *et al.* 2014). Moreover, DELLA proteins act as negative regulators that inhibit plant growth by modulating the GA signaling pathway (Brian *et al.* 1967). Active GA binds to *GID1* in plants, which leads to the degradation of DELLA proteins *via* the ubiquitin-proteasome system. This degradation results in the loss of DELLA protein function and the subsequent regulation of downstream genes (Chevreau and Leblay 1993; Daviere and Achard 2016). Therefore, exploring the key genes involved in GA anabolism and signal transduction is crucial for enhancing crop yields.

While numerous genes regulating internode length have been identified across various crops, research specifically focusing on the genes governing internode length in tomato remains limited. Previous studies indicate that the *dwarf* (*D*) gene encodes a critical enzyme within the brassinosteroid (BR) biosynthetic pathway, thereby regulating internode length through the modulation of BR synthesis (Montoya *et al.* 2005). This gene is the first identified in tomato that affects internode length. Furthermore, mutations in the *PRO* gene (Jupe *et al.* 1988), which is associated with DELLA proteins and promotes GA synthesis, have been shown to extend tomato internodes. Recently, the role of GA synthesis genes in shaping tomato plant architecture has been increasingly documented. For example, mutations in *SlGA2ox7* inhibit the degradation of GA, resulting in the accumulation of active GA species and the emergence of naturally occurring long internode mutants *El* and *tie-1* (Schrager-Lavelle *et al.* 2019; Sun *et al.* 2019). Additionally, *SlDREB* negatively regulates the expression of enantiocopalyl diphosphate synthetase (*SlCPS*) and *GA20 oxidase* (*SlGA20ox1/2/4*). The overexpression of *SlDREB* inhibits the normal biosynthesis of GAs, leading to reduced endogenous GA levels and restricting the elongation of tomato internodes (Li *et al.* 2012). Investigating the key genes involved in the biosynthesis and signaling mechanisms of GA is essential for regulating tomato growth and development, enhancing tomato yield, and improving the overall quality of tomatoes.

A substantial number of studies have contributed to a foundational understanding of the internodal regulatory mechanisms in grass crops. However, there remains considerable scope for further research on internode development in *Solanaceae* crops. In this study, we identified a tomato elongated internode mutant, *tei*, which arose from natural field mutations in high-generation tomato inbred lines. Through phenotypic analysis, we observed that *tei* exhibits longer internodes and darker leaf coloration. Subsequently, we crossed the long internode mutant *tei* with WT, which displays normal internode length, to create genetic populations (F_1 and F_2). We conducted genetic mapping and transcriptome-assisted validation to identify the primary candidate gene *TEI*. Furthermore, we evaluated various studies through endogenous hormone determination, expression analysis, and phylogenetic assessment to support the hypothesis that *TEI* may play a crucial role in regulating tomato internode elongation. To further elucidate the function of *TEI*, we employed CRISPR/Cas9 technology to construct *TEI* mutants. The resulting mutants exhibited shorter internodes compared to WT. These findings will contribute to the development of a theoretical framework for understanding the molecular mechanisms underlying tomato internode regulation.

2. Materials and methods

2.1. Plant materials and growth conditions

This study utilized a field elongated internode (*tei*) mutant derived from a high-generation inbred line of tomato. The *tei* mutant served as the male parent, while the wild type (WT), characterized by normal internode length, functioned as the female parent. These two lines were crossed to generate F_1 and F_2 populations, which were subsequently employed for gene mapping and genetic analysis. All tomato plants were cultivated in a controlled temperature environment at 25°C, with photoperiodic conditions maintained under cool white fluorescent lights following a 16:8 L/D cycle. The 35-d-old parental plants and their progeny were transplanted into the greenhouse at Xiangyang Farm, Northeast Agricultural University, China, over a span of three consecutive years. Throughout this period, standard practices for water and fertilizer management, as well as scientific measures for pest and disease control, were rigorously applied. Additionally, tobacco (*Nicotiana benthamiana*) (Goodin *et al.* 2008) materials were grown in a growth chamber under a 16:8 L/D cycle for a duration of 5 to 6 weeks. All materials utilized in this study were provided by the Tomato Research Institute of Northeast Agricultural University, China.

2.2. Histological staining

The third internode of both *tei* and WT plants, which were cultivated for 45 d, was selected for paraffin sectioning. Stem segments, approximately 5 mm in size, were collected and immersed in FAA fixative solution at a volume 20 times that of the tissue block, followed by fixation at room temperature for 24 h. The samples were then softened in a 50% glycerol solution for one week, after which they were dehydrated using ethanol solutions of increasing concentrations (70 to 100%). Subsequently, the samples were treated with xylene solution and embedded in wax. Continuous wax strips were cut using a Leica rotary microtome (RM2125, Leica Biosystems, Germany). After spreading, the sections were deparaffinized, stained with Safranin O-Fast Green, and sealed with neutral gum before being examined under a light microscope.

2.3. Scanning electron microscope (SEM) observation

The fifth true leaves of *tei*, WT and F_1 plants cultured for 45 and 75 d were selected, washed with deionized water, cut into small pieces, and fixed in 2.5% glutaraldehyde at pH 6.8. After washing the samples three times with phosphate buffer, they were dehydrated using a series of ethanol concentrations. Subsequently, the samples were treated with a 1:1 solution of 100% ethanol and tert-butanol, and then with pure tert-butanol, and then frozen at –20°C for 30 min. A 15-nm thick gold layer was deposited on the dried samples using an ES-2030 ion sputtering coating machine from Hitachi (ES-2030, Hitachi, Japan). Finally, the samples were examined under a scanning electron microscope (S-3400) and photographed for further analysis.

2.4. Transmission electron microscopy (TEM) observation

The fifth true leaves of *tei*, WT and F_1 plants cultured for 45 and 75 d were selected, fixed in glutaraldehyde for one week, and then washed three times with phosphate buffer (pH 6.8) at 4°C. Subsequently, the samples were fixed in 1% osmium tetroxide for 3 h. After rinsing three times with phosphate buffer, the samples were dehydrated using a 1:1 mixture of 100% ethanol and acetone, and finally immersed in n-propanol. The samples were then embedded in a mixture of acetone and epoxy resin before being polymerized at 60°C in a constant-temperature incubator. Ultrathin sections (50–60 nm) were prepared using an ULTRACUT-E ultramicrotome from Reichert-Jung (ULTRACUT-E, Reichert-Jung, Austria). These sections were stained with a binary solution of uranyl acetate and lead citrate at 25°C, and subsequently observed and photographed using an H-7650 transmission electron microscope manufactured by Hitachi (H-7650, Hitachi, Japan).

2.5. Extraction and quantification of endogenous GAs

Young leaf samples of the *tei* mutant and WT, weighing 0.2 g each, were selected for analysis. Initially, methanol was added, followed by petroleum ether for repeated extraction and decolorization. Subsequently, triethylamine and polyvinylpolypyrrolidone (PVPP) were incorporated, and the mixture was extracted with ethyl acetate to facilitate phase integration of the esters. After evaporating the solution to dryness under reduced pressure at 0°C, the mobile phase solution was introduced, and the residue was dissolved through vortexing and shaking. The solution was then filtered using a needle filter. The liquid chromatography conditions for quantifying endogenous GAs were as follows: a Shimadzu LC-20AT equipped with a UV detector (SPD-20A), a column oven (CTO-20AC), and a C18 reversed-phase column (150 mm×4.6 mm, 5 μm). The mobile phase consisted of A: 100% methanol and B: 0.1% acetic acid aqueous solution, in a ratio of A:B=55:45. The injection volume was 20 μL, the flow rate was set at 0.8 mL min^{-1}, the column temperature was maintained at 30°C, and the UV wavelength was 254 nm.

2.6. Chlorophyll and photosynthesis determination

We measured *tei* and the fifth true leaf of WT 45 d after planting using a portable photosynthesis measurement system (Li-6400, LI-COR, USA). Measurements were taken between 9:00 and 9:30 AM and included net photosynthetic rate, intercellular CO_2 concentration, and SPAD values. For each species, five plants were selected, and the averages were calculated. The reference method for determining chlorophyll content is based on the work of Yu *et al.* (2021), which provides a reliable and accurate measurement of chlorophyll content.

2.7. Analysis of genetic patterns and BSA-seq

We recorded mean internode length data for P_1 (*tei*) (n=12), P_2 (WT) (n=12), F_1 (n=24), and F_2 populations (n=303), measured according to the method described by Martí *et al.* (2006). The average length of the five internodes from the first to the fifth inflorescence was calculated. Statistical analyses were conducted using Microsoft® Excel 2016 and SPSS 23.0, with the coefficient of variation (CV%) calculated using the formula $CV\%=\sigma/\mu\times100\%$, where σ represents the standard deviation and μ represents the mean value. Additionally, a frequency distribution histogram of the F_2 population was plotted using GraphPad Prism 8. Thirty extremely long and thirty extremely short plants were selected as materials to construct designated extreme hybrid pools, referred to as “f2c” and “f2d,” respectively. Three plants from each parental line, P_1 and P_2, were selected to construct a parental internode length library. Approximately 0.2 g of young leaves per plant were sent to BGI (Shenzhen, China) for subsequent library construction. Whole-genome resequencing was performed using the BGISEQ platform (Fang *et al.* 2018), and raw data were filtered using Soapnuke software. Using the tomato genome SL4.0 (ftp://ftp.solgenomics.net/tomato_genome/annotation/ITAG4.0_release) as the reference genome for resequencing, BWA was employed to align the short sequences obtained from second-generation sequencing with the reference genome. SNP variation within the population was detected using GATK3.4 software. By calculating the allele depth of the parent pool-offspring pool, the SNP-index result is obtained, and then the data is filtered and plotted through the sliding window method.

2.8. CAPS marker, InDel marker development and MassARRAY SNP genotyping and genetic mapping

InDel markers were designed using 500 bp sequences from upstream and downstream base deletion/insertion sites, based on resequencing results and inter-parental sequence polymorphisms. Single nucleotide polymorphisms (SNPs) were extracted, and Primer5.0 software was employed to identify the appropriate cleavage sites. The SNP sites were subsequently converted into cleaved amplified polymorphic sequence (CAPS) sites, resulting in the development of CAPS molecular markers. Primers were designed using the NCBI Primer-BLAST online tool (https://www.ncbi.nlm.nih.gov/tools/primer-blast/) and Primer 5.0 software. In this study, six restriction enzymes were utilized: *BsaAI*, *HpaI*, *AfeI*, *AuaI*, *TaqI*, and *Eco130I*. MassARRAY SNP genotyping, a flight mass spectrometry-based technology, was employed to develop SNP markers within the flanking marker intervals, informed by genetic mapping results of the tomato long internode spacer gene (Appendix A). Leaf DNA was extracted from 300 plants of the F_2 population and sent to BGI (Shenzhen, China) for SNP genotyping; the resulting genotyping data were subsequently used to encrypt the markers. Statistical analysis of the genotyping data was conducted using Microsoft® Excel 2016. The primer sequences corresponding to the markers are presented in Appendix A. Based on the band results obtained through gel electrophoresis and associated phenotypic data, JoinMap4 mapping software was utilized to construct a genetic map of the F_2 mapping population. Genetic distances were calculated using genetic frequencies (rfs) and Kosambi mapping functions. Following this, genetic analysis of individual F_2 plants was performed using flanking markers to identify recombinant plants and refine candidate intervals for the elongated internode trait.

2.9. RNA extraction and expression analysis

Total RNA was extracted from the root, stem, leaf, bud, flower, and fruit tissues of tomato using the FreeZol Reagent (#R711) extraction kit. The extracted total RNA was then reverse transcribed into cDNA. This was done using the HiS III RT SuperMix for qPCR (+gDNA wiper) reagent from Vazyme. Quantitative reverse transcription-PCR (qRT-PCR) analysis was conducted using SYBR Green reagent (Guenin *et al.* 2009). The relative expression of the gene was calculated employing the $2^{-\Delta\Delta CT}$ method, and all qPCR analyses were performed with three biological replicates and three technical replicates. A Student's *t*-test was conducted using SPSS 23.0. This was done to compare the expression of *TEI* within the same tissue between the two materials, and also to compare the expression of the homologous *SlGA20ox1-4* gene in the stem internodes of the two materials. Specific primer information is provided in Appendix B.

2.10. Subcellular localization

We utilized CE Design V1.04 software to design primers for homologous recombination. The *TEI* coding sequence, after removing the stop codon, was cloned using KOD One PCR Master Mix (TOYOBO). The *pC1300s-GFP* vector was linearized using FastDigest (Thermo Scientific), and the target fragment was inserted between *Kpn*I and *Bam*HI sites with the ClonExpress II one-step cloning kit (Vazyme), thereby completing the construction of the *35S::TEI-GFP* fusion vector. The bacterial solution was injected into the distal axial end of tobacco leaves as described by Liu *et al.* (2024). After the injection, the tobacco leaves were kept in the dark for 12 h. They were then subjected to a standard incubation period of 48 h. Subsequently, *GFP* fluorescence was observed using a laser confocal microscope (FV3000, Olympus, Japan). The primers utilized in this study are detailed in Appendix B.

2.11. Bioinformatics analysis

The tertiary structure of the TEI protein was modeled using homology modeling with the online tool Phyre2 (http://www.sbg.bio.ic.ac.uk/phyre2/html/page.cgi?id=index), and the resulting structure was visualized in PyMOL v3.1.0 after obtaining the corresponding PDB file. Homologous genes from tomato and other species were identified by submitting the TEI amino acid sequences to NCBI's BLASTP search program (https://blast.ncbi.nlm.nih.gov/Blast.cgi). The protein sequences were subsequently downloaded and analyzed using ESPript 3.0 (https://espript.ibcp.fr/ESPript/cgi-bin/ESPript.cgi) for homologous sequence comparison (Parmagnani *et al.* 2022). The MEGA11 software was employed to construct the phylogenetic tree using the Neighbour Joining method (Tamura *et al.* 2021). The protein structural domains of TEI were predicted using the Conserved Domains feature from the InterPro database (Mulder *et al.* 2007) (https://www.ebi.ac.uk/interpro/). Additionally, the *cis*-acting elements of the promoter were analyzed through the PlantCARE (Lescot *et al.* 2002) online tool (http://bioinformatics.psb.ugent.be/webtools/plantcare/html/).

2.12. Analysis of RNA-Seq data

We performed RNA sequencing analysis of tomato stem internodes (*tei* and WT) 45 d after transplantation. All tomato samples were collected from three biological replicates, each comprising 10 plants. Libraries were constructed using total RNA and sequenced on the Illumina HiSeq 2000 platform (Caporaso *et al.* 2012). The tomato genome version SL4.0 was obtained from the SOL Genomics Network (http://solgenomics.net/). The RNA-Seq data were analysed according to previously established protocols (Yang *et al.* 2024).

2.13. Accession numbers

The sequence data referenced in this paper are accessible through the SGN (https://solgenomics.net/) databases. The corresponding accession numbers are as follows: *TEI* (*Solyc09g042210*), *SlGA20ox1* (*Solyc03g006880*), *SlGA20ox2* (*Solyc06g035530*), *SlGA20ox3* (*Solyc11g072310*), *SlGA20ox4* (*Solyc01g093980*), and actin (*Solyc03g078400*).

3. Results

3.1. Mutant *tei* has longer internode

The plant mutant *tei* was derived from a natural mutation in

the high-generation inbred tomato line WT. The *tei* mutant exhibited a greater plant height compared to WT (Fig. 1-A). However, there was no significant difference in the number of internodes between the two. To elucidate the reason for the observed difference in plant height, we measured the lengths of the first to fifth internodes of *tei*, WT, and F_1 (Fig. 1-B). The results indicated that, in comparison to WT, each internode of *tei* and F_1 was longer (Table 1), and the average internode length of *tei* and F_1 was significantly greater than that of WT (Fig. 1-C and D). Consequently, we selected the third internode, which exhibited the most pronounced length difference, to prepare paraffin sections for examining the cell morphology of *tei* and WT. Microscopic images clearly demonstrated that the cell length of the longitudinal sections of the *tei* internode was significantly larger than that of the WT internode (Fig. 1-G and H). The statistical analysis results confirmed this finding (Fig. 1-F). This suggests that the internode elongation observed in *tei* mutants could be attributed to the elongation of cells within the stem. Furthermore, we conducted a comparative analysis of the

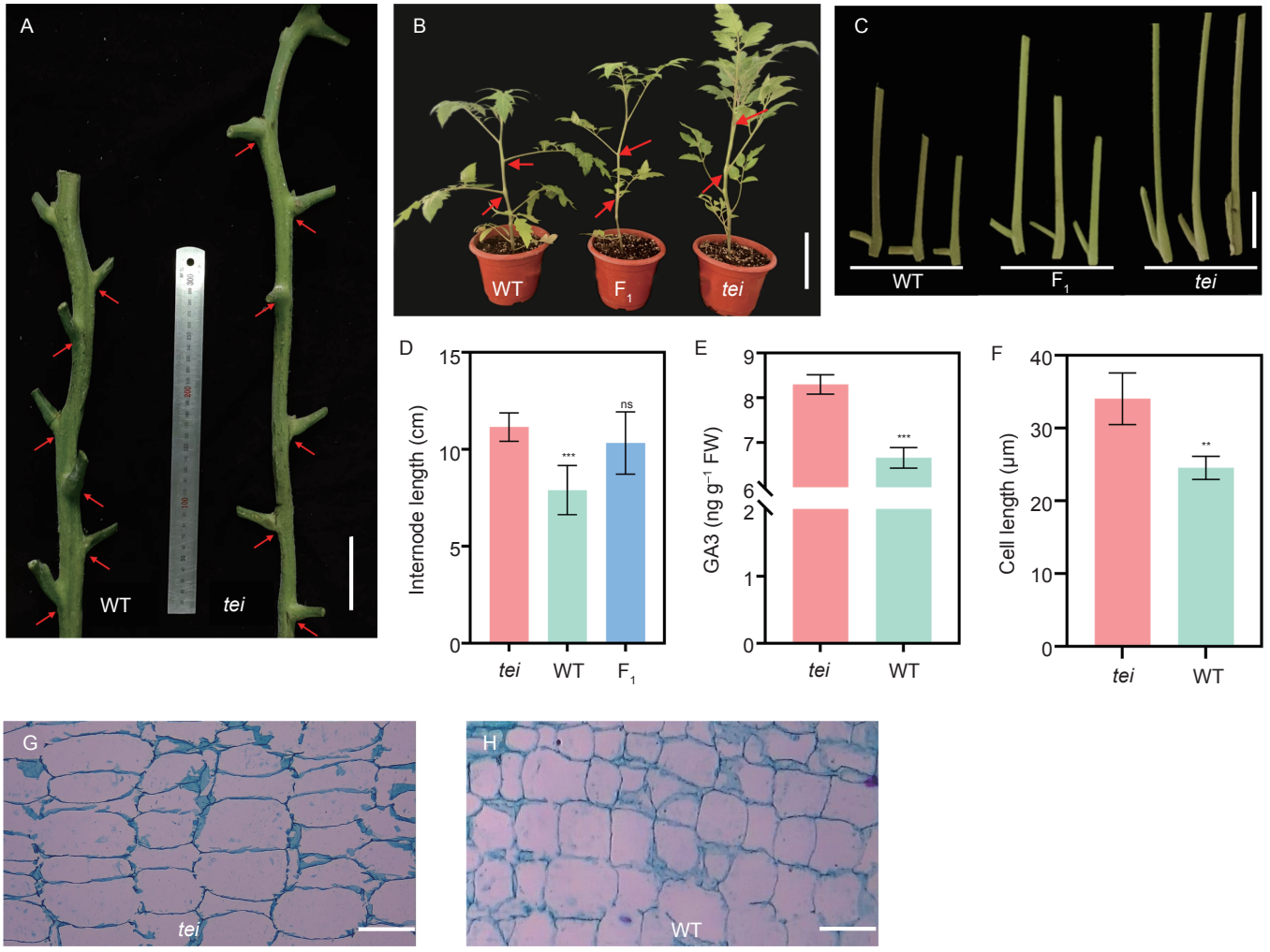


Fig. 1 Phenotypic analysis of the long internode mutant *tei* compared to the normal internode WT. A, five internode length phenotypes of *tei* and WT. B and C, internode characteristics of *tei*, WT, and their F_1. D, internode length statistics for *tei*, WT, and F_1. E, comparison of endogenous GA3 content in *tei* and WT. F, statistical data of cell length in G and H. G and H, longitudinal anatomical sections of the third internodal stems of *tei* and WT. D was analyzed for significance using one-way ANOVA, while E and F were tested for significance using Student's *t*-test. ***, $P<0.001$; **, $P<0.01$; ns>0.05. Data are mean±SD ($n=8$). Scale bars in A, B, C, G and H represent 8 cm, 15 cm, 1 cm, 20 μm, and 20 μm, respectively.

Table 1 Average length of each internode from the first to the fifth internode

Generations	1st internode (cm)	2nd internode (cm)	3rd internode (cm)	4th internode (cm)	5th internode (cm)
tei (P_1)	10.75±1.39 a	12.83±3.42 a	12.29±2.86 a	10.58±2.15 a	9.29±2.15 ab
WT (P_2)	7.87±1.24 b	8.96±2.46 b	7.29±3.31 b	7.62±2.46 b	7.75±2.45 b
F_1	9.87±2.13 a	11.37±3.5 ab	10.46±3.77 a	11.3±4.11 a	10.27±3.09 a

Data are mean±SD ($n=8$). Letters following the values indicate the significance of differences in the same internode length among the different materials, which were comparatively analyzed using the one-way ANOVA method.

endogenous GA3 content in *tei* and WT after 35 d of growth and discovered that the GA3 content in *tei* was significantly higher than that in WT (Fig. 1-E). Therefore, the internode elongation phenotype observed in *tei* may be associated with cell elongation resulting from the accumulation of elevated levels of bioactive GA3.

3.2. Mutant *tei* has darker leaves and stronger photosynthesis

Phenotypic observations indicated that, compared to WT, the *tei* mutant not only exhibited longer internodes but also displayed a darker leaf color. To investigate the underlying cause of the dark green color of *tei* leaves and its impact on photosynthetic organisms, we selected the fifth main leaves from *tei*, WT and F_1 plants derived from *tei* and WT at 45 and 72 d post-transplantation for TEM and SEM analyses. The results demonstrated that at 45 d after cultivation, the chloroplast lamellae of both plants were neatly arranged, showing no significant differences. However, the palisade parenchyma and spongy tissues of *tei* were larger than those of WT (Fig. 2-B and D). At 72 d after cultivation, we observed that the chloroplast lamellar structure of WT had decomposed, while the chloroplast structure of *tei* remained intact; additionally, the thickness of both the palisade and spongy tissues in *tei* was still greater than that of WT (Fig. 2-A and C). Therefore, the increased thickness of the palisade parenchyma in *tei*, along with the integrity of its chloroplast structure, accounts for the dark green color of the leaves. We subsequently measured the chlorophyll content, SPAD value, intercellular CO_2 concentration, and net photosynthetic rate of *tei*, WT, and their F_1 progeny at 45 and 72 d after cultivation (Fig. 2-E–L). The results indicated that the chlorophyll content and net photosynthetic rate of *tei* were higher than those of WT. In summary, *tei* exhibited a deeper leaf color and enhanced photosynthetic capacity.

3.3. RNA-seq enrichment of the GA pathway

We conducted transcriptome sequencing of *tei* and WT plants, identifying a total of 292 differentially expressed genes, which included 131 up-regulated and 161 down-regulated genes (Fig. 3-A). Subsequent KEGG enrichment analysis revealed significant enrichment in the pathways involved in GA synthesis and photosynthesis (Appendix C). These findings are consistent with our previous phenotypic analyses and physiological measurements. Furthermore, we characterized the GA pathway, which can be primarily divided into the GA synthesis pathway and the signal transduction pathway (Fig. 3-B). Within the GA synthesis pathway, *GA20ox* and *GA3ox* serve as key enzymes for GA synthesis, while *GA2ox* plays a crucial role in regulating GA degradation (Fig. 3-C). Collectively, these enzymes facilitate the synthesis of active GAs (GA1 and GA4) from GGPP, while the binding of active GA to GID1 induces conformational changes in the DELLA protein, leading to its degradation and thereby promoting the accumulation of GAs.

3.4. Evaluation of F_2 populations

The internode phenotype of the F_2 population, derived from a cross between *tei* and WT, was characterized. The results indicated that the average internode length of the 303 F_2 hybrids was 11.16 cm which was significantly closer to that of *tei*. A statistical analysis was performed on the average internode length, length range, coefficient of variation (CV%), kurtosis (K), and skewness (S) across the four generations: P_1, P_2, F_1, and F_2 (Appendix D). Notably, the variation range of internode length in the male parent (*tei*) was the smallest, while the hybrid F_2 exhibited the largest variation range. The coefficient of variation, which reflects the degree of population dispersion, was lowest in the sire group. Analyzing the internode length data of F_2 revealed a continuous distribution, with the highest frequency of internode lengths occurring around 12 cm (Fig. 4-A). Furthermore, the absolute values of skewness and kurtosis for the F_2 population were both less than 1, indicating that the data conform to a normal distribution and align with the characteristics of quantitative traits.

3.5. BSA-seq and fine mapping of *TEI*

Initially, BSA-seq was conducted (Appendices E and F), revealing a distinct separation region on chromosome 9 that encompasses the *TEI* interval (Fig. 4-B). We designated the primary locus influencing internode length as *qEIN9.1*. Utilizing resequencing data, we genotyped 303 F_2 monocultures using 8 InDel markers to construct a genetic map for the *qEIN9.1* locus. By analyzing the internode phenotypes of individual F_2 plants, we determined that the *qEIN9.1* locus is located between InDel-332 and InDel-556, with genetic distances of 1.2 and 0.8 cM to these markers, respectively. The flanking markers, InDel-332 and InDel-556 (Fig. 4-C), were employed to screen 1,000 F_2 recombinants, leading to the identification of 10 recombinant strains. These 10 recombinant individuals were further genotyped using 6 CAPS markers and 3 SNP markers. By integrating the phenotypic data from the recombinants, the internodal *qEIN9.1* locus was ultimately narrowed down to the region between markers CAPS55 and SNP21, which corresponds to a physical distance of 150 kb (Fig. 4-D and E). According to reference genome information, there exists only one candidate gene within this interval, namely *Solyc09g042210.1.1*. The full length of this gene is 617 bp, with a coding sequence (CDS) of 393 bp, consisting of 2 exons and 1 intron, and is associated with GA synthase *GA20ox* (Fig. 4-F). Based on the fine mapping results, this gene is proposed as a potential candidate for regulating internode elongation, and we designated it as *TEI*.

3.6. Expression and phylogenetic analysis of *TEI*

We cloned the *TEI* gene from the *tei* mutant, and sequencing analysis revealed no non-synonymous mutations in the coding sequence of the *TEI* gene. However, within the first 2,000 bp of the promoter region, we identified 123 SNP mutations and 6 InDel mutations, including a 24 bp insertion at position 1,035 bp (Fig. 5-E). Predictions of *cis*-acting elements indicated that the mutations introduced into the *TEI* promoter region resulted in the formation of five CAAT boxes and two TATA boxes, which may influence promoter

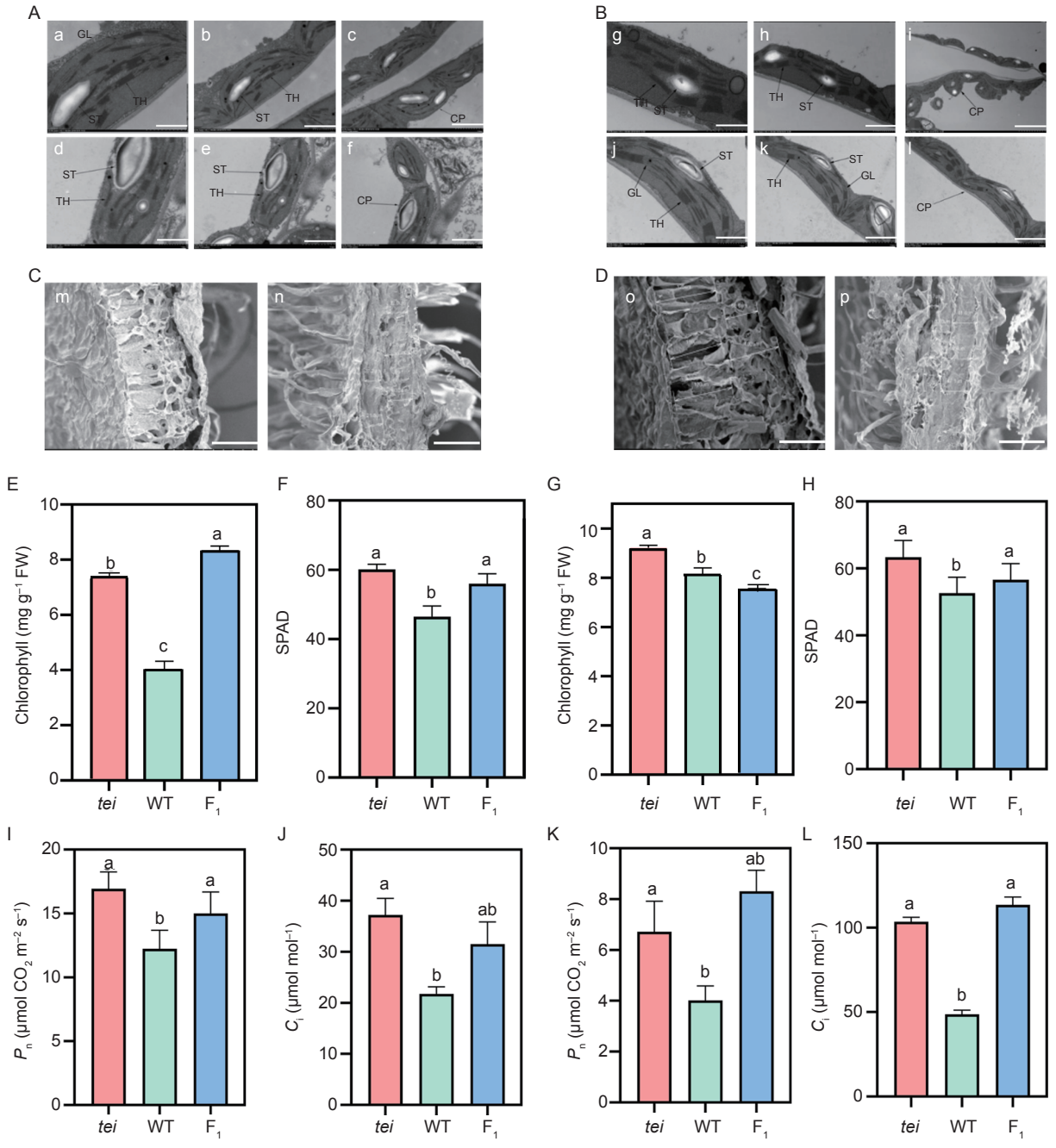


Fig. 2 Electron microscopy images of blade structures and physiological measurements of samples *tei* and WT. A and B, transmission electron microscopy images of WT (a, b, c) and *tei* (g, h, i) chloroplasts cultivated for 45 d, as well as WT (d, e, f) and *tei* (j, k, l) chloroplasts cultivated for 72 d. C and D, scanning electron microscopy images of leaf tissues from WT (m) and *tei* (o) plants cultivated for 45 d, alongside WT (n) and *tei* (p) plants cultivated for 72 d. E–H, chlorophyll content and SPAD values were measured for WT, *tei*, and F_1 at 45 d of cultivation (E and F) and 72 d of cultivation (G and H). I–L, net photosynthetic rate and intercellular CO_2 concentration for WT, *tei*, and F_1 were measured at 45 and 72 d of cultivation. All results are presented as means±SD (n=5 plants). Lowercase letters (a, b, c) indicate statistically significant differences according to two-way ANOVA and Tukey's multiple comparison test. Scale bars in panels A and B represent 50 μm for a, d, g, j; 100 μm for b, e, h, k; and 500 μm for c, f, i, l, while those in panels C and D represent 100 μm, respectively. CP, chloroplast; GL, grana lamellae; TH, thallus; ST, starch grain.

activity and alter the transcription levels of *TEI* (Appendix G). To investigate the tissue specificity of the *TEI* gene, we conducted qRT-PCR analysis on the roots, stems, leaves, buds, flowers, and fruits of both *tei* and WT at maturity (Fig. 5-A). The results demonstrated that the *TEI* gene was expressed in all developmental stages of both materials, with significantly higher expression levels observed in the stems of *tei* compared to WT. To further explore the functional site of *TEI*, we constructed a *35S::TEI-GFP* reporter system and transiently transformed it into tobacco (Fig. 5-B). Fluorescence imaging revealed that *TEI* signals were detected in both the plasma membrane and the cytoplasm. Through homology modeling and sequence alignment, we found that the TEI protein is homologous to four typical

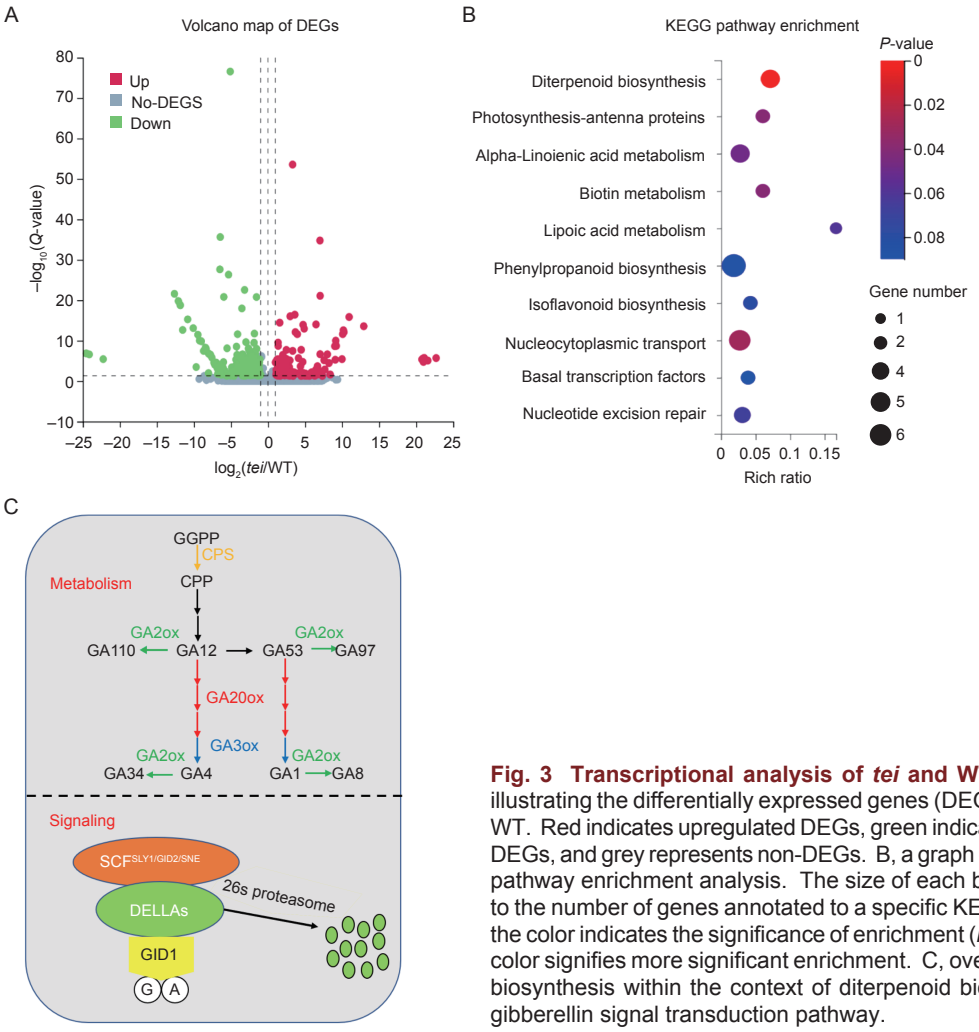


Fig. 3 Transcriptional analysis of *tei* and WT. A, volcano plot illustrating the differentially expressed genes (DEGs) between *tei* and WT. Red indicates upregulated DEGs, green indicates downregulated DEGs, and grey represents non-DEGs. B, a graph depicting the KEGG pathway enrichment analysis. The size of each bubble corresponds to the number of genes annotated to a specific KEGG pathway, while the color indicates the significance of enrichment (*P*-value); darker red color signifies more significant enrichment. C, overview of gibberellin biosynthesis within the context of diterpenoid biosynthesis and the gibberellin signal transduction pathway.

GA20ox proteins (*SlGA20ox1–4*), all of which contain the conserved 2OG-FeII_Ox domain responsible for catalytic activity (Fig. 5-C). To further investigate the phylogenetic relationship of TEI, homologous alignment of TEI protein sequences was performed. The results indicated that the TEI protein exhibited high similarity to the potato protein XP_006357721.1, which encodes a GA 20-oxidase gene (Fig. 5-D).

3.7. Knocking out *TEI* leads to shorter internode

To further investigate the biological function of *TEI*, we employed CRISPR/Cas9 gene editing technology to introduce mutations in the *TEI* locus. Two specific target sites were designed within the first and second exons. The mutations in the *TEI* gene were subsequently verified through sequencing following *Agrobacterium tumefaciens*-mediated transformation. We isolated two distinct homozygous mutant lines, *CR-tei5* and *CR-tei9* from the T_1 generation for further analysis. An 8-bp base deletion was identified at the first target site of the *TEI* locus in *CR-tei5*, whereas a 2-bp deletion was observed in *CR-tei9* (Fig. 6-A). Base deletion analysis revealed that, compared to WT, both *CR-tei5* and *CR-tei9* experienced premature transcription termination following the deletions, resulting in a reduction in the number of amino acids and alterations to the protein structure. We then conducted quantitative real-time PCR to assess the expression levels of *TEI* in the *CR-tei* mutant lines (Fig. 6-D). Notably, the *TEI* transcript was nearly completely silenced in these mutants. These results confirm the successful mutation of *TEI*. In addition, observing the mutants 30 d after transplantation compared to WT plants, both *CR-tei5* and *CR-tei9* mutants exhibited shorter fruit internode length (Fig. 6-B). Phenotypic analysis revealed that the internode length of the *tei* mutant significantly differed from that of the WT. Statistical analysis further confirmed the role of the *TEI* gene in promoting internode elongation (Fig. 6-C and E). In summary, knockout of the *TEI* gene results in shortened plant internode length, thus confirming the regulatory effect of this gene on internode length.

4. Discussion

Optimizing plant structure is the primary strategy for increasing tomato yield. Plant height is a critical economic trait in tomatoes, primarily determined by the number and length of internodes (Cho *et al.* 2016). Genes such as the mutant *self-pruning* (*sp*) (Magome *et al.* 2004), the *semi-determinant* gene (*sdt*) (Elkind *et al.* 1991), and the *sp suppressor* gene (*ssp*) (Park *et al.* 2014) indirectly influence the number of internodes, while flowering signals regulate plant dwarfing. However, most variation in plant height is

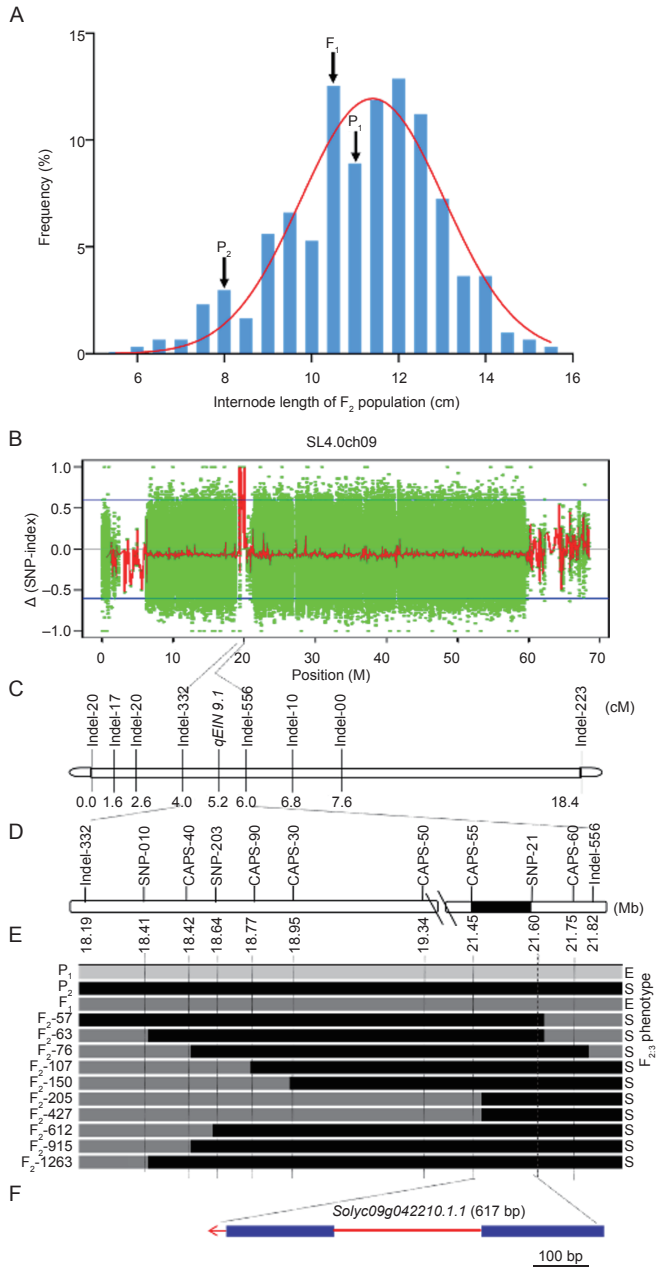


Fig. 4 Mapping clones of the *qEIN9.1* primary effector locus. A, frequency histogram of internode length for 303 F_2 monocots. B, the Δ(SNP-index) plot of chromosome 9 was generated using the Δ(SNP-index) based algorithm in BSA-seq. The red line illustrates the fitted ΔSNP-index, and the blue line denotes the 99% confidence interval derived from the *t*-test. C, a genetic map of *qEIN9.1* is presented. A small F_2 population (n=303 was utilized to narrow the interval between Indel-332 and Indel-556 using InDel markers. D and E, fine mapping of the *qEIN9.1* locus was conducted. New markers were developed to analyze larger F_2 populations (n=1,000) and 10 recombinant lines, successfully locating the *qEIN9.1* locus between two flanking markers, CAPS-55 and SNP-21 (E represents the long internode phenotype, and S represents the short internode phenotype). F, within the candidate interval, a candidate gene encoding *GA20ox* was identified within the 150 kb candidate range.

attributed to changes in internode length. The long internode tomato mutants *El* and *tie-1* (Schrager-Lavelle *et al.* 2019; Sun *et al.* 2019) and the dwarf mutants *d*, *br*, and *si* (Bishop *et al.* 1996; Gao *et al.* 2018; Kwon *et al.* 2020) have all demonstrated that these genes affect plant height through modifications in internode length. Therefore, the localization, cloning, and identification of key genes regulating internodes will accelerate their application in tomato breeding and significantly enhance our understanding of the mechanisms underlying internode elongation.

In this study, we observed that the average internode length in the *tei* population increased by 48.7% compared to WT, while the number of internodes remained unchanged (Fig. 1-A–D, Table 1). This indicates that the phenotypes associated with plant height mutations are primarily due to the elongation of internodes. GAs are crucial in regulating internode length. Previous research has demonstrated that GA biosynthesis pathway is impaired in the cucumber dwarf mutant *cp-3* , leading to inhibited cell division and elongation (Sun *et al.* 2024). Our analysis of longitudinal structural sections of stem internodes revealed that the node cells in long internode mutants are significantly elongated. Furthermore, endogenous GA3 was detected in both samples, with the content of active GA3 in *tei* being significantly higher than that in WT (Fig. 1-E). Overall, we conclude that elevated levels of active GA promote cell elongation, resulting in internode elongation. During the characterization of the internode length phenotype, we found that the *tei* mutant exhibits elongated internodes, deeper leaf color, and enhanced light-harvesting ability (Fig. 1). Physiological assessments and electron microscopy observations indicated that *tei* possesses dark green leaves and enhanced photosynthetic capacity, with transcriptomic analysis also revealing enrichment in photosynthetic pathways (Figs. 2 and 3). Notably, we discovered that *tei* exhibits a more compact plant structure and a significantly smaller leaf angle compared to WT (Appendix H). Previous studies have shown that plant height can co-localize with various relevant traits, including flowering time, tiller number (Hart *et al.* 2001; Niu *et al.* 2022; Tian *et al.* 2022) and seed weight (Feltus *et al.* 2006). However, it remains unclear whether the genetic mechanisms underlying simultaneous mutations in plant height and leaf angle are attributable to a single gene or the interactions between multiple genes that affect the pleiotropy of different traits (Yang *et al.* 2023). Additionally, an examination of other agronomic traits among the three lines revealed that *tei* and F_1 hybrids exhibited a shorter maturation period and higher yield compared to WT (Appendix I). We hypothesize that these observations may be attributed to increased internode length, reduced leaf angle, and the presence of dark green leaf color.

To clarify the cause of internode elongation, *tei* mutants were crossed with WT plants to establish F_2 and $F_{2:3}$ populations for genetic analysis of internode length. Preliminary phenotypic investigations indicated that the internode length of the F_2 population exhibited a normal distribution, reflecting the fundamental characteristics of quantitative traits (Fig. 4-A). Initially, we employed BSA-seq for preliminary mapping, followed by a map cloning approach to identify the primary effect sites of *qEIN9.1*. Ultimately, we identified the gene *Solyc09g042210* (*TEI*) as our candidate gene (Fig. 4-B–F). However, we did not detect non-synonymous mutations in the

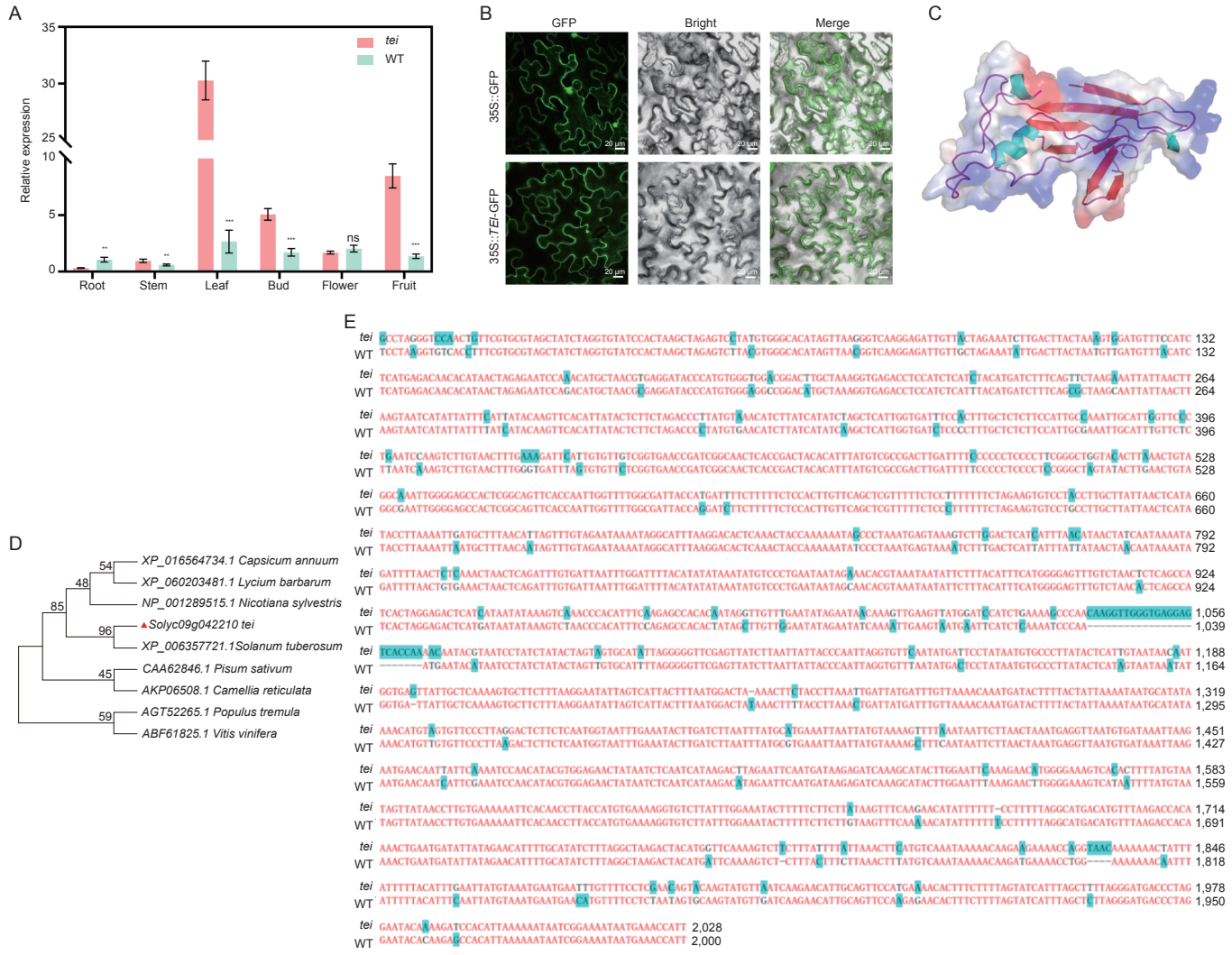


Fig. 5 Expression analysis, promoter mutation, and phylogenetic tree construction of *TEI*. A, relative expression of the *TEI* gene in various tissues from *tei* and WT materials. Significance analyses were conducted using Student's *t*-test, with results indicating ***, $P<0.001$; **, $P<0.01$, and ns for non-significant. B, subcellular localization of *TEI-GFP* in tobacco, with *35S::GFP* serving as a blank control. The scale bar indicates 20 μm. C, a 3D model of the TEI protein, where red arrows represent β-folds, blue long curls denote α-helices, blue short curls indicate η-helices, and purple lines illustrate random curls. D, phylogenetic analysis of TEI protein. E, comparison of promoter sequencing of *TEI* in *tei* and WT, with red letters representing consistent bases and blue regions denoting bases with different types of mutations.

coding region of the *TEI* gene; instead, we identified numerous mutations in the promoter region (Fig. 5-E). These findings prompted us to further investigate the potential impact of these promoter mutations. Numerous studies have demonstrated that alterations in cis-acting elements can modify gene expression and lead to changes in plant morphology (Arnaud *et al.* 2011). A 20 bp deletion in the *GA3ox* promoter of the natural short internode mutant *si-2* impedes transcription and results in reduced GA content (Anarjan *et al.* 2023). Many mutations in the *TEI* promoter region induce changes in *cis*-regulatory elements, which may alter the activity of the *TEI* promoter and subsequently affect *TEI* expression or signal transduction. Expression analyses revealed that *TEI* was expressed in all tissues, with significantly higher expression levels in *tei* mutant stems compared to WT (Fig. 5-A). A total of four classical *GA20ox* genes were compared by aligning the *TEI* gene with their tomato homologues (Fig. 5-D, Appendix J). Compared to WT, the expression levels of *SlGA20ox1-4* in the *tei* mutant stem nodes were significantly increased (Appendix K). This finding further corroborates the elevated active GA content observed in *tei* mutants. Additionally, characterization of the *TEI* protein structure indicated that *TEI* is classified as a *GA20ox* gene (Fig. 5-C). As a GA synthase, *GA20ox* sequentially catalyzes the conversion of inactive GA into active GA at the final stage of GA biosynthesis (Fukazawa *et al.* 2017; Zheng *et al.* 2019). Sequence alignment of the TEI protein revealed that the potato protein XP_006357721.1, which encodes *GA20ox1*, exhibited the highest structural similarity. Furthermore, overexpression of *StGA20ox1* has been shown to enhance plant height and root length in potato.

Therefore, we propose that *Solyc09g042210* is the primary regulatory gene for *tei* internode mutations; however, its mechanism of action warrants further investigation and

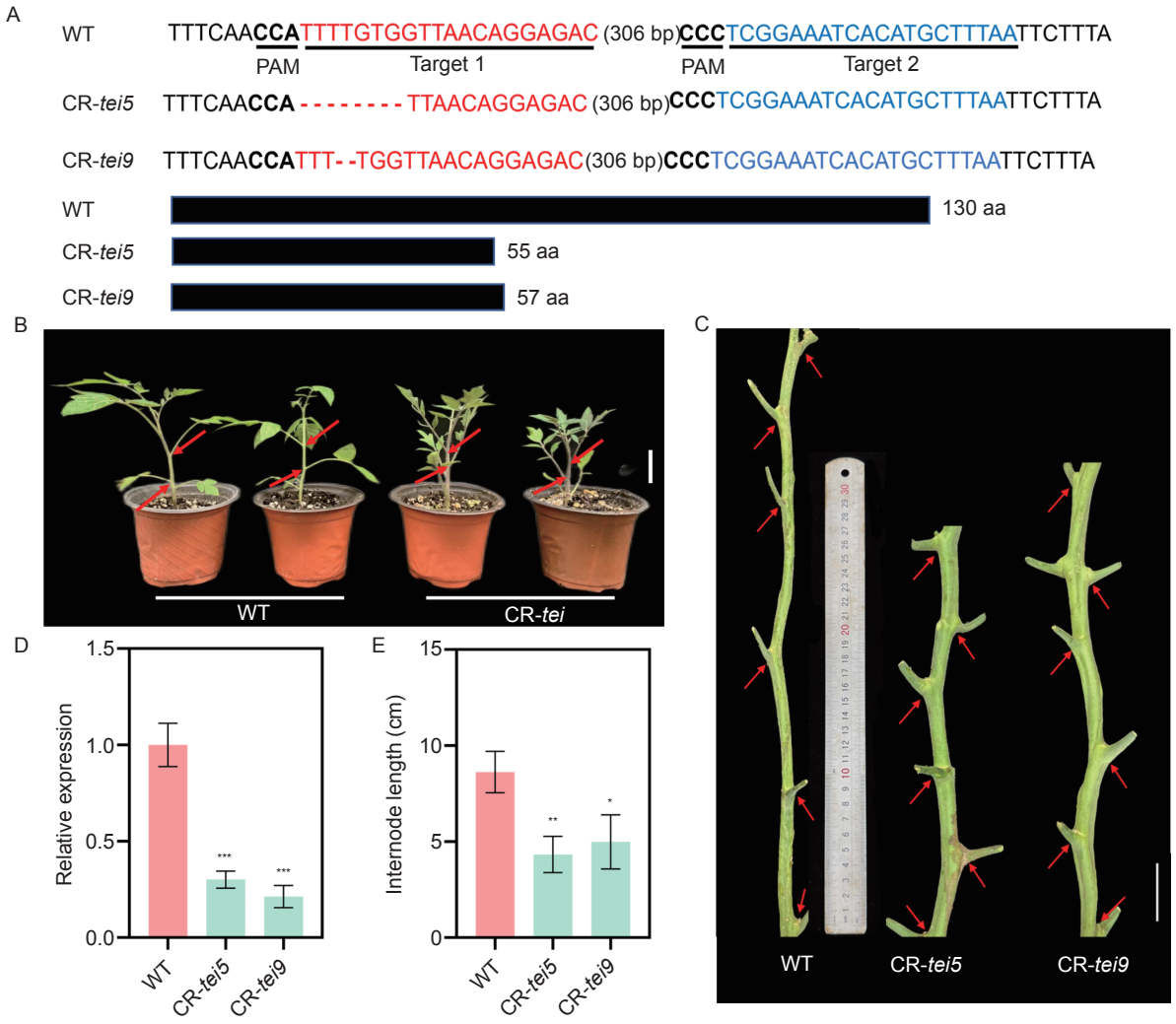


Fig. 6 Knockdown of the *TEI* gene resulted in shorter internodes. A, the *TEI* site mutant genotypes were generated using the CRISPR/Cas9 genome editing system. The two recognition sites for the protospacer adjacent motif (PAM) are indicated in bold, while the sequences for target 1 and target 2 are highlighted in red and blue letters, respectively. Mutations in the transgenic plants were confirmed by sequencing the genomic regions flanking the target sites. The sequences from WT plants and two homozygous mutant lines (CR-*tei5* and CR-*tei9*) are presented. B and C, phenotypic analysis of WT and homozygous mutants CR-*tei5* and CR-*tei9* (scale bars represent 5 and 4 cm). D, relative expression levels of the *TEI* gene in WT and homozygous mutants CR-*tei5* and CR-*tei9*. E, the average internode length statistics of WT and CR-*tei5*, CR-*tei9* (D and E were analyzed for significance using Student's *t*-test; ***, $P<0.001$; **, $P<0.01$; *, $P<0.05$.). Data are mean±SD ($n=5$).

elucidation. To further confirm that *TEI* is the principal gene regulating tomato internode length. To directly test this hypothesis, we employed CRISPR/Cas9 technology to knock out this gene in WT tomato plants. After gene editing, base deletions and frameshift mutations were observed, resulting in premature termination of transcription. Phenotypic observations indicated that *CR-tei5* and *CR-tei9* exhibited reduced internode lengths compared to WT. Consequently, we conclude that the *TEI* gene is a key regulator of internode length in tomato.

5. Conclusion

In this study, we identified a tomato *tei* mutant exhibiting elongated internodes, which was caused by increased GA levels and enhanced stem cell elongation. The candidate gene *TEI* (*Solyc09g042210*) encodes a GA20ox protein, and promoter variations result in its elevated expression in the mutant. *TEI* is the key regulator of internode elongation and represents a promising target for improving tomato plant architecture through GA regulation.

Acknowledgements

This study was support by the grants from the Natural Science Foundation of Heilongjiang Province, China (YQ2024C010); the Key Research and Development Plan of Heilongjiang Province, China (SC2022ZX02C0202); CARS (CARS-23-A11) and the Hainan Province "Nanhai Xinxing" Science and Technology Innovation Talent Platform Project, China (NHXXRCXM202333).

Declaration of competing interest

The authors declare that they have no conflict of interest.

Declaration of generative AI and AI-assisted technologies in the writing process

The authors declare that they did not use AI in the preparation and writing of this manuscript.

Appendices associated with this paper are available at https://doi.org/10.1016/j.jia.2025.12.055

References

Anarjan M B, Begum S, Bae I, Lee S. 2023. Mutation in the *GA3ox* gene governs short-internode characteristic in a Korean cucumber inbred line. *Horticulture*, *Environment*, *and Biotechnology*, **64**, 485–495.

Arnaud N, Lawrenson T, Østergaard L, Sablowski R. 2011. The same regulatory point mutation changed seed-dispersal structures in evolution and domestication. *Current Biology*, **21**, 1215–1219.

Berry P, Sterling M, Spink J, Baker C, Sylvester-Bradley R, Mooney S, Tams A, Ennos A. 2004. Understanding and reducing lodging in cereals. *Advances in Agronomy*, **84**, 215–269.

Bishop G J, Harrison K, Jones J. 1996. The tomato *Dwarf* gene isolated by heterologous transposon tagging encodes the first member of a new cytochrome P450 family. *The Plant Cell*, **8**, 959–969.

Brian P, Grove J F, Mulholland T. 1967. Relationships between structure and growth-promoting activity of the gibberellins and some allied compounds, in four test systems. *Phytochemistry*, **6**, 1475–1499.

Caporaso J G, Lauber C L, Walters W A, Berg-Lyons D, Huntley J, Fierer N, Owens S M, Betley J, Fraser L, Bauer M. 2012. Ultra-high-throughput microbial community analysis on the Illumina HiSeq and MiSeq platforms. *The ISME Journal*, **6**, 1621–1624.

Chen Y, Hou M, Liu L, Wu S, Shen Y, Ishiyama K, Kobayashi M, McCarty D R, Tan B C. 2014. The maize *DWARF1* encodes a gibberellin 3-oxidase and is dual localized to the nucleus and cytosol. *Plant Physiology*, **166**, 2028–2039.

Chevreau E, Leblay C. 1993. The effect of mother plant pretreatment and explant choice on regeneration from *in vitro* pear leaves. *Acta Horticulturae*, **336**, 263–268.

Cho S H, Kang K, Lee S H, Lee I J, Paek N C. 2016. *OsWOX3A* is involved in negative feedback regulation of the gibberellic acid biosynthetic pathway in rice (*Oryza sativa*). *Journal of Experimental Botany*, **67**, 1677–1687.

Daviere J M, Achard P. 2016. A pivotal role of DELLAs in regulating multiple hormone signals. *Molecular Plant*, **9**, 10–20.

Elkind Y, Gurnick A, Kedar N. 1991. Genetics of semideterminate growth habit in tomato. *HortScience*, **26**, 1074–1075.

Fang C, Zhong H, Lin Y, Chen B, Han M, Ren H, Lu H, Luber J M, Xia M, Li W. 2018. Assessment of the cPAS-based BGISEQ–500 platform for metagenomic sequencing. *Gigascience*, **7**, gix133.

Fang Q, Zhang X, Chen S, Shao L, Sun H, Yan Z. 2019. Selecting traits to reduce seasonal yield variation of summer maize in the North China Plain. *Agronomy Journal*, **111**, 343–353.

Feltus F, Hart G, Schertz K, Casa A, Kresovich S, Abraham S, Klein P, Brown P, Paterson A. 2006. Alignment of genetic maps and QTLs between inter- and intra-specific *sorghum* populations. *Theoretical and Applied Genetics*, **112**, 1295–1305.

Fukazawa J, Mori M, Watanabe S, Miyamoto C, Ito T, Takahashi Y. 2017. *DELLA-GAF1* complex is a main component in gibberellin feedback regulation of GA20 oxidase 2. *Plant Physiology*, **175**, 1395–1406.

Gao Z, Feng H Y, Liang X G, Zhang L, Lin S, Zhao X, Shen S, Zhou L L, Zhou S L. 2018. Limits to maize productivity in the North China Plain: A comparison analysis for spring and summer maize. *Field Crops Research*, **228**, 39–47.

Goodin M M, Zaitlin D, Naidu R A, Lommel S A. 2008. *Nicotiana benthamiana*: Its history and future as a model for plant–pathogen interactions. *Molecular Plant–Microbe Interactions*, **21**, 1015–1026.

Guenin S, Mauriat M, Pelloux J, Van Wuytswinkel O, Bellini C, Gutierrez L. 2009. Normalization of qRT-PCR data: The necessity of adopting a systematic, experimental conditions-specific, validation of references. *Journal of Experimental Botany*, **60**, 487–493.

Hart G, Schertz K, Peng Y, Syed N. 2001. Genetic mapping of *Sorghum bicolor* (L.) Moench QTLs that control variation in tillering and other morphological characters. *Theoretical and Applied Genetics*, **103**, 1232–1242.

Ishikawa S, Maekawa M, Arite T, Onishi K, Takamure I, Kyozuka J. 2005. Suppression of tiller bud activity in tillering dwarf mutants of rice. *Plant and Cell Physiology*, **46**, 79–86.

Ji S, Gururani M, Lee J, Ahn B O, Chun S C. 2014. Isolation and characterisation of a dwarf rice mutant exhibiting defective gibberellins biosynthesis. *Plant Biology*, **16**, 428–439.

Jupe S, Causton D, Scott I. 1988. Cellular basis of the effects of gibberellin and the *pro* gene on stem growth in tomato. *Planta*, **174**, 106–111.

Khush G S. 1999. Green revolution: Preparing for the 21st century. *Genome*, **42**, 646–655.

Khush G S. 2001. Green revolution: The way forward. *Nature Reviews Genetics*, **2**, 815–822.

Kieffer M, Master V, Waites R, Davies B. 2011. *TCP14* and *TCP15* affect internode length and leaf shape in *Arabidopsis*. *The Plant Journal*, **68**, 147–158.

Kwon C T, Heo J, Lemmon Z H, Capua Y, Hutton S F, Van Eck J, Park S J, Lippman Z B. 2020. Rapid customization of *Solanaceae* fruit crops for urban agriculture. *Nature Biotechnology*, **38**, 182–188.

Lescot M, Déhais P, Thijs G, Marchal K, Moreau Y, Van de Peer Y, Rouzé P, Rombauts S. 2002. PlantCARE, a database of plant *cis*-acting regulatory elements and a portal to tools for *in silico* analysis of promoter sequences. *Nucleic Acids Research*, **30**, 325–327.

Li J, Li C, Smith S M. 2017. *Hormone Metabolism and Signaling in Plants*. Academic Press, United States.

Li J, Sima W, Ouyang B, Wang T, Ziaf K, Luo Z, Liu L, Li H, Chen M, Huang Y. 2012. Tomato *SlDREB* gene restricts leaf expansion and internode elongation by downregulating key genes for gibberellin biosynthesis. *Journal of Experimental Botany*, **63**, 6407–6420.

Liu L, Zhao L, Liu Y, Zhu Y, Chen S, Yang L, Li X, Chen W, Xu Z, Xu P. 2024. Transcription factor *OsWRKY72* controls rice leaf angle by regulating *LAZY1*-mediated shoot gravitropism. *Plant Physiology*, **195**, 1586–1600.

Magome H, Yamaguchi S, Hanada A, Kamiya Y, Oda K. 2004. *Dwarf and delayed-flowering 1*, a novel *Arabidopsis* mutant deficient in gibberellin biosynthesis because of overexpression of a putative *AP2* transcription factor. *The Plant Journal*, **37**, 720–729.

Martí E, Gisbert C, Bishop G J, Dixon M S, García-Martínez J L. 2006. Genetic and physiological characterization of tomato cv. Micro-Tom. *Journal of Experimental Botany*, **57**, 2037–2047.

Montoya T, Nomura T, Yokota T, Farrar K, Harrison K, Jones J G, Kaneta T, Kamiya Y, Szekeres M, Bishop G J. 2005. Patterns of *Dwarf* expression and brassinosteroid accumulation in tomato reveal the importance of brassinosteroid synthesis during fruit development. *The Plant Journal*, **42**, 262–269.

Mulder N J, Apweiler R, Attwood T K, Bairoch A, Bateman A, Binns D, Bork P, Buillard V, Cerutti L, Copley R. 2007. New developments in the InterPro database. *Nucleic Acids Research*, **35**, D224–D228.

Niu M, Wang H, Yin W, Meng W, Xiao Y, Liu D, Zhang X, Dong N, Liu J, Yang Y. 2022. Rice *DWARF AND LOW-TILLERING* and the homeodomain protein OSH15 interact to regulate internode elongation via orchestrating brassinosteroid signaling and metabolism. *The Plant Cell*, **34**, 3754–3772.

Olszewski N, Sun T P, Gubler F. 2002. Gibberellin signaling: Biosynthesis, catabolism, and response pathways. *The Plant Cell*, **14**, S61–S80.

Paciorek T, Chiapelli B J, Wang J Y, Paciorek M, Yang H, Sant A, Val D L, Boddu J, Liu K, Gu C. 2022. Targeted suppression of gibberellin biosynthetic genes *ZmGA20ox3* and *ZmGA20ox5* produces a short stature maize ideotype. *Plant Biotechnology Journal*, **20**, 1140–1153.

Park S J, Jiang K, Tal L, Yichie Y, Gar O, Zamir D, Eshed Y, Lippman Z B. 2014. Optimization of crop productivity in tomato using induced mutations in the florigen pathway. *Nature Genetics*, **46**, 1337–1342.

Parmagnani A S, D'Alessandro S, Maffei M E. 2022. Iron-sulfur complex assembly: Potential players of magnetic induction in plants. *Plant Science*, **325**, 111483.

Schrager-Lavelle A, Gath N N, Devisetty U K, Carrera E, López-Díaz I, Blazquez M A, Maloof J N. 2019. The role of a class III gibberellin 2-oxidase in tomato internode elongation. *The Plant Journal*, **97**, 603–615.

Sun X, Shu J, Ali Mohamed A M, Deng X, Zhi X, Bai J, Cui Y, Lu X, Du Y,

Wang X. 2019. Identification and characterization of *El* (*Elongated Internode*) gene in tomato (*Solanum lycopersicum*). *International Journal of Molecular Sciences*, **20**, 2204.

Sun Y, Zhou K, Wang X, Li X, Zhang X, Han N, Zhang J, Chen S. 2024. Identification and characterization of *CsERECTA*, a major gene controlling stem elongation through regulating GA biosynthesis in cucumber. *Theoretical and Applied Genetics*, **137**, 151.

Tamura K, Stecher G, Kumar S. 2021. MEGA11: Molecular evolutionary genetics analysis version 11. *Molecular Biology and Evolution*, **38**, 3022–3027.

Tian Y, Yang L, Lu H, Zhang B, Li Y, Liu C, Ge T, Liu Y, Han J, Li Y, Qiu L. 2022. QTL analysis for plant height and fine mapping of two environmentally stable QTLs with major effects in soybean. *Journal of Integrative Agriculture*, **21**, 933–946.

Wang S, Wang Y. 2022. Harnessing hormone gibberellin knowledge for plant height regulation. *Plant Cell Reports*, **41**, 1945–1953.

Xue W, Xing Y, Weng X, Zhao Y, Tang W, Wang L, Zhou H, Yu S, Xu C, Li X. 2008. Natural variation in *Ghd7* is an important regulator of heading date and yield potential in rice. *Nature Genetics*, **40**, 761–767.

Yamaguchi M, Fujimoto H, Hirano K, Araki-Nakamura S, Ohmae-Shinohara K, Fujii A, Tsunashima M, Song X J, Ito Y, Nagae R. 2016. *Sorghum Dw1*, an agronomically important gene for lodging resistance, encodes a novel protein involved in cell proliferation. *Scientific Reports*, **6**, 28366.

Yan P, Zhu Y, Wang Y, Ma F, Lan D, Niu F, Dong S, Zhang X, Hu J, Liu S. 2022. A new RING finger protein, PLANT ARCHITECTURE and GRAIN NUMBER 1, affects plant architecture and grain yield in rice. *International Journal of Molecular Sciences*, **23**, 824.

Yang H, Zhou K, Wu Q, Jia X, Wang H, Yang W, Lin L, Hu X, Pan B, Li P. 2024. The tomato *WRKY-B* transcription factor modulates lateral branching by targeting *BLIND*, *PIN4*, and *IAA15*. *Horticulture Research*, **11**, uhae193.

Yang X, Li R, Jablonski A, Stovall A, Kim J, Yi K, Ma Y, Beverly D, Phillips R, Novick K. 2023. Leaf angle as a leaf and canopy trait: Rejuvenating its role in ecology with new technology. *Ecology Letters*, **26**, 1005–1020.

Yu Y, Qi Y, Xu J, Dai X, Chen J, Dong C H, Xiang F. 2021. *Arabidopsis WRKY71* regulates ethylene-mediated leaf senescence by directly activating *EIN2*, *ORE1* and *ACS2* genes. *The Plant Journal*, **107**, 1819–1836.

Zhang Y, Zhang B, Yan D, Dong W, Yang W, Li Q, Zeng L, Wang J, Wang L, Hicks L M. 2011. Two *Arabidopsis* cytochrome P450 monooxygenases, *CYP714A1* and *CYP714A2*, function redundantly in plant development through gibberellin deactivation. *The Plant Journal*, **67**, 342–353.

Zheng L, Gao C, Zhao C, Zhang L, Han M, An N, Ren X. 2019. Effects of brassinosteroid associated with auxin and gibberellin on apple tree growth and gene expression patterns. *Horticultural Plant Journal*, **5**, 93–108.

Executive Editor-in-Chief Sanwen Huang
Managing Editor Lingyun Weng